Mon. Not. R. Astron. Soc. **000**, 1–10 (2009) Printed February 19, 2009 (MN LaTeX style file v2.2)

Compressed sensing imaging techniques for radio interferometry

Y. Wiaux[1,2], L. Jacques[1,3], G. Puy[1], A. M. M. Scaife[4], P. Vandergheynst[1]
[1]*Institute of Electrical Engineering, Ecole Polytechnique Fédérale de Lausanne (EPFL), CH-1015 Lausanne, Switzerland*
[2]*Centre for Particle Physics and Phenomenology, Université catholique de Louvain (UCL), B-1348 Louvain-la-Neuve, Belgium*
[3]*Communications and Remote Sensing Laboratory, Université catholique de Louvain (UCL), B-1348 Louvain-la-Neuve, Belgium*
[4]*Astrophysics Group, Cavendish Laboratory, University of Cambridge, Cambridge CB3 0HE, United Kingdom*

February 19, 2009

ABSTRACT
Radio interferometry probes astrophysical signals through incomplete and noisy Fourier measurements. The theory of compressed sensing demonstrates that such measurements may actually suffice for accurate reconstruction of sparse or compressible signals. We propose new generic imaging techniques based on convex optimization for global minimization problems defined in this context. The versatility of the framework notably allows introduction of specific prior information on the signals, which offers the possibility of significant improvements of reconstruction relative to the standard local matching pursuit algorithm CLEAN used in radio astronomy. We illustrate the potential of the approach by studying reconstruction performances on simulations of two different kinds of signals observed with very generic interferometric configurations. The first kind is an intensity field of compact astrophysical objects. The second kind is the imprint of cosmic strings in the temperature field of the cosmic microwave background radiation, of particular interest for cosmology.

Key words: techniques: interferometric, techniques: image processing, cosmology: cosmic microwave background

1 INTRODUCTION

Radio interferometry is a powerful technique for aperture synthesis in astronomy, dating back to more than sixty years ago (Ryle & Vonberg 1946; Blythe 1957; Ryle et al. 1959; Ryle & Hewish 1960; Thompson et al. 2004). In a few words, thanks to interferometric techniques, radio telescope arrays synthesize the aperture of a unique telescope of the same size as the maximum projected distance between two telescopes on the plane perpendicular to the pointing direction of the instrument. This allows observations with otherwise inaccessible angular resolutions and sensitivities in radio astronomy. The small portion of the celestial sphere accessible to the instrument around the pointing direction tracked during observation defines the original real planar signal or image I to be recovered. The fundamental Nyquist-Shannon theorem requires a signal to be sampled at a frequency of twice its bandwidth to be exactly known. The signal I may therefore be expressed as a vector $x \in \mathbb{R}^N$ containing the required number N of sampled values. Radio-interferometric data are acquired in the Fourier plane. The number m of spatial frequencies probed may be much smaller than the number N of discrete frequencies of the original band-limited signal, so that the Fourier coverage is incomplete. Moreover the spatial frequencies probed are not uniformly sampled. The measurements are also obviously affected by noise. An ill-posed inverse problem is thus defined for reconstruction of the original image.

Beyond the Nyquist-Shannon theorem, the emerging theory of compressed sensing aims at merging data acquisition and compression (Candès et al. 2006a,b; Candès 2006; Donoho 2006; Baraniuk 2007). It notably relies on the idea that a large variety of signals in Nature are sparse or compressible. By definition, a signal is sparse in some basis if its expansion contains only a small number of non-zero coefficients. More generally it is compressible if its expansion only contains a small number of significant coefficients, i.e. if a large number of its coefficients bear a negligible value. Compressed sensing theory demonstrates that a much smaller number of linear measurements is required for accurate knowledge of such signals than is required for Nyquist-Shannon sampling. The sensing matrix must simply satisfy a so-called restricted isometry property. In particular, a small number of random measurements in a sensing basis incoherent with the sparsity or compressibility basis will ensure this property with overwhelming probability, e.g. random Fourier measurements of a signal sparse in real or wavelet space. Consequently, if compressed sensing had been developed before the advent of radio interferometry, one could probably not have thought of a much better design of measurements for sparse and compressible signals in an imaging perspective.

In this work we present results showing that the theory of compressed sensing offers powerful image reconstruction techniques for radio-interferometric data. These techniques are based on global minimization problems, which are solved by convex optimization algorithms. We also emphasize on the versatility of the scheme relative to the inclusion of specific prior information on the signal in the minimization problems. This versatility allows the definition of image reconstruction techniques which are significantly more powerful than standard deconvolution algorithm called CLEAN used in the context of radio astronomy.

In Section 2, we pose the inverse problem for image reconstruction from radio-interferometric data and discuss the standard image reconstruction techniques used in radio astronomy. In Section 3, we concisely describe the central results of the theory of compressed sensing regarding the definition of a sensing basis and the accurate reconstruction of sparse or compressible signals. In Section 4, we firstly comment on the exact compliance of radio interferometric measurements with compressed sensing. We then study the reconstruction performances of various compressed sensing imaging techniques relative to CLEAN on simulations of two kinds of signals of interest for astrophysics and cosmology. We finally conclude in Section 5.

Notice that a first application of compressed sensing in astronomy (Bobin et al. 2008) was very recently proposed for non-destructive data compression on board the future Herschel space observatory[1]. The versatility of the compressed sensing framework to account for specific prior information on signals was already pointed out in that context. Moreover, the generic potential of compressed sensing for interferometry was pointed in the signal processing community since the time when the theory emerged (Donoho 2006; Candès et al. 2006b; Mary & Michel 2007; Levanda & Leshem 2008). It was also very recently acknowledged in radio astronomy (Cornwell 2008). The present work nonetheless represents the first application of compressed sensing for the definition of new imaging techniques in radio interferometry. A huge amount of work may be envisaged along these lines, notably for the transfer of the proposed techniques to optical and infrared interferometry. The extension of these techniques from the plane to the sphere will also be essential, notably with regard to forthcoming radio interferometers with wide fields of view on the celestial sphere (Cornwell et al. 2008; McEwen & Scaife 2008), such as the future Square Kilometer Array (SKA)[2] (Carilli & Rawlings 2004).

2 RADIO INTERFEROMETRY

In this section, we recall the van Cittert-Zernike theorem on the basis of which we formulate the inverse problem posed for image reconstruction from radio-interferometric data. We also describe and discuss the standard image reconstruction techniques used in radio astronomy, namely a local matching pursuit algorithm called CLEAN and a global optimization algorithm called the maximum entropy method (MEM).

2.1 van Cittert-Zernike theorem

In a tracking configuration, all radio telescopes of an interferometric array point in the same direction. The field of view observed on the celestial sphere S^2 is limited by a so-called illumination function $A(\omega)$, depending on the angular position $\omega \in \mathrm{S}^2$. The size of its angular support is essentially inversely proportional to the size of the dishes of the telescopes (Thompson et al. 2004). At each instant of observation, each telescope pair identified by an index b measures a complex visibility $y_b \in \mathbb{C}$. This visibility is defined as the correlation between incoming electric fields E at the positions of the two telescopes in the three-dimensional space, $\vec{b}_1, \vec{b}_2 \in \mathbb{R}^3$:

$$y_b = \left\langle E\left(\vec{b}_1, t\right) E^*\left(\vec{b}_2, t\right) \right\rangle_{\Delta t}. \tag{1}$$

In this relation, t denotes the time variable and the brackets $\langle \cdot \rangle_{\Delta t}$ denote an average over a time Δt long relative to the period of the radio wave detected.

We consider a monochromatic signal with a wavelength of emission λ, and made up of incoherent sources. We also consider a standard interferometer with an illumination function whose angular support is small enough so that the field of view may be identified to a planar patch of the celestial sphere: $P \subset \mathbb{R}^2$. The signal and the illumination function thus respectively appear as functions $I(\vec{p})$ and $A(\vec{p})$ of the angular variable seen as a two-dimensional vector $\vec{p} \in \mathbb{R}^2$ with an origin at the pointing direction of the array. The vector $\vec{B}_b = \vec{b}_2 - \vec{b}_1 \in \mathbb{R}^3$ defining the relative position between the two telescopes is called the baseline, and its projection on the plane perpendicular to the pointing direction of the instrument may be denoted as $\vec{B}_b^{\perp} \in \mathbb{R}^2$. One also makes the additional assumption that the maximum projection of the baselines in the pointing direction itself is small (Cornwell et al. 2008). In this context, the so-called van Cittert-Zernike theorem states that the visibility measured identifies with the two-dimensional Fourier transform of the image multiplied by the illumination function AI at the single spatial frequency

$$\vec{u}_b = \frac{\vec{B}_b^{\perp}}{\lambda}, \tag{2}$$

i.e.

$$y_b = \widehat{AI}\left(\vec{u}_b\right), \tag{3}$$

with

$$\widehat{AI}\left(\vec{u}\right) \equiv \int_{\mathbb{R}^2} A\left(\vec{p}\right) I\left(\vec{p}\right) e^{-2i\pi\vec{p}\cdot\vec{u}} \mathrm{d}^2\vec{p}, \tag{4}$$

for any two-dimensional vector $\vec{u} \in \mathbb{R}^2$. Interferometric arrays thus probe signals at a resolution equivalent to that of a single telescope with a size R essentially equivalent to the maximum projected baseline on the plane perpendicular to the pointing direction: $R \simeq \max_b \vec{B}_b^{\perp}$. This expresses the essence of aperture synthesis (Thompson et al. 2004).

2.2 Interferometric inverse problem

In the course of an observation, the projected baselines on the plane perpendicular to the pointing direction change thanks to the Earth's rotation and run over an ellipse in the Fourier plane of the original image, whose parameters are linked to the parameters of observation. The total number $m/2$ of spatial frequencies probed by all pairs of telescopes of the array during the observation provides some Fourier coverage characterizing the interferometer. Any interferometer is thus simply identified by a binary mask in Fourier equal to 1 for each spatial frequency probed and 0 otherwise. The visibilities measured may be denoted as a vector of $m/2$ complex Fourier coefficients $y \in \mathbb{C}^{m/2} = \{y_b = \widehat{AI}(\vec{u}_b)\}_{1 \leqslant b \leqslant m/2}$, possibly affected by complex noise values $n \in \mathbb{C}^{m/2} = \{n_b = n(\vec{u}_b)\}_{1 \leqslant b \leqslant m/2}$ of astrophysical or instrumental origin. Considering that the signal I and the illumination function A are real, a symmetry $\widehat{AI}(-\vec{u}_b) = \widehat{AI}^*(\vec{u}_b)$ also holds so that independent measurements may all be localized in one half of the Fourier

[1] http://herschel.esac.esa.int/
[2] http://www.skatelescope.org/

plane. The binary mask in Fourier identifying the interferometer is defined in this half of the plane and rendered symmetric around the origin so that it also corresponds to the Fourier transform of a real function. In this context, the measured visibilities may equivalently be denoted as a vector of m real Fourier coefficients $y \in \mathbb{R}^m = \{y_r\}_{1\leqslant r\leqslant m}$ consisting of the real and imaginary parts of the complex measures, possibly affected by real noise values $n \in \mathbb{R}^m = \{n_r\}_{1\leqslant r\leqslant m}$.

The original signal $I(\vec{p})$ and the illumination function $A(\vec{p})$ can be approximated by band-limited functions restricted to the finite field of view precisely set by the illumination function: $\vec{p} \in P$. In this context, we notice that they are identified by their Nyquist-Shannon sampling on a discrete uniform grid of $N = N^{1/2} \times N^{1/2}$ points $\vec{p}_i \in \mathbb{R}^2$ in real space with $1 \leqslant i \leqslant N$. The sampled signal may thus be denoted as $x \in \mathbb{R}^N = \{x_i = I(\vec{p}_i)\}_{1\leqslant i\leqslant N}$ while the illumination function is denoted as $a \in \mathbb{R}^N = \{a_i = A(\vec{p}_i)\}_{1\leqslant i\leqslant N}$, and the sampled product reads as $\bar{x} \in \mathbb{R}^N = \{\bar{x}_i = AI(\vec{p}_i)\}_{1\leqslant i\leqslant N}$. Because of the assumed finite field of view, the functions may equivalently be described by their complex Fourier coefficients on a discrete uniform grid of $N = N^{1/2} \times N^{1/2}$ spatial frequencies $\vec{u}_i$ with $1 \leqslant i \leqslant N$. This grid is symmetric around the origin and limited at the maximum frequency defining the band limit. In particular for the Fourier coefficients of the product AI one has: $\widehat{\bar{x}} \in \mathbb{C}^N = \{\widehat{\bar{x}}_i = \widehat{AI}(\vec{u}_i)\}_{1\leqslant i\leqslant N}$. The functions being real, one again has the symmetry $\widehat{AI}(-\vec{u}_i) = \widehat{AI}^*(\vec{u}_i)$ so that the signal is described by exactly $N/2$ complex Fourier coefficients in one half of the Fourier plane, or equivalently N real Fourier coefficients consisting of the real and imaginary parts of these complex coefficients. In the following we only use this decomposition with real coefficients in one half of the Fourier plane.

However the frequencies $\vec{u}_b$ probed defined by (2) for $1 \leqslant b \leqslant m/2$ are continuous and do not generally belong to the set of discrete frequencies $\vec{u}_i$ for $1 \leqslant i \leqslant N$. Reconstruction schemes in general perform a preliminary gridding operation on the visibilities y_r with $1 \leqslant r \leqslant m$ so that the inverse problem may be reformulated in a pure discrete setting, i.e. between the discrete Fourier and real planes (Thompson et al. 2004). The essential reason for the gridding resides in the subsequent use of the standard fast Fourier transform (FFT)[3]. For the sake of the considerations that follow we assume that the frequencies probed $\vec{u}_b$ belong to the discrete grid of points $\vec{u}_i$ so that no artifact due to the gridding is introduced. In this discrete setting the Fourier coverage is unavoidably incomplete in the sense that the number of real constraints m is always smaller than the number of unknowns N: $m < N$. An ill-posed inverse problem is thus defined for the reconstruction of the signal x from the measured visibilities y as:

$$y = \Phi_{\mathrm{ri}} x + n, \tag{5}$$

for a given noise n, and with a sensing matrix Φ_{ri} for radio interferometry of the form

$$\Phi_{\mathrm{ri}} = MFD. \tag{6}$$

In this relation, the matrix $D \in \mathbb{R}^{N\times N} = \{D_{ii'} = a_i\delta_{ii'}\}_{1\leqslant i,i'\leqslant N}$ is the diagonal matrix implementing the illumination function, and the matrix $F \in \mathbb{R}^{N\times N} = \{F_{ii'}\}_{1\leqslant i,i'\leqslant N}$ implements the discrete Fourier transform providing the real Fourier coefficients in one half of the Fourier plane. The matrix $M \in \mathbb{R}^{m\times N} = \{M_{ri}\}_{1\leqslant r\leqslant m;1\leqslant i\leqslant N}$ is the rectangular binary matrix implementing the mask characterizing the interferometer in one half of the Fourier plane. It contains only one non-zero value on each line, at the index of one of the two real Fourier coefficients corresponding to each of the spatial frequencies probed.

[3] Notice that fast algorithms have been developed to compute a Fourier transform on non-equispaced spatial frequencies (NFFT) (Potts et al. 2008). This could in principle allow one to avoid an explicit gridding operation.

We restrict our considerations to independent Gaussian noise with variance $\sigma_r^2 = \sigma^2(y_r)$. From a statistical point of view, the likelihood $\mathcal{L}$ associated with a candidate reconstruction x^* of the signal x is defined as the probability of the data y given the model x^*, or equivalently the probability of the noise residual $n^* = y - \Phi_{\mathrm{ri}} x^*$. Under the Gaussian noise assumption it reads as

$$\mathcal{L}\left(y|x^*\right) \propto \exp\left[-\frac{1}{2}\chi^2\left(x^*;\Phi_{\mathrm{ri}},y\right)\right], \tag{7}$$

with the corresponding negative logarithm

$$\chi^2\left(x^*;\Phi_{\mathrm{ri}},y\right) = \sum_{r=1}^{m}\frac{\left(n_r^*\right)^2}{\sigma_r^2}, \tag{8}$$

following a chi-square distribution with m degrees of freedom. The χ^2 defines a noise level estimator. The level of residual noise n^* should be reduced by finding x^* minimizing this χ^2, which corresponds to maximize the likelihood $\mathcal{L}$. Typically, the measurement constraint on the reconstruction may be defined as a bound

$$\chi^2\left(x^*;\Phi_{\mathrm{ri}},y\right) \leqslant \epsilon^2, \tag{9}$$

with ϵ^2 corresponding to some $(100\alpha)^{\mathrm{th}}$ percentile of the chi-square distribution, i.e. $p(\chi^2 \leqslant \epsilon^2) = \alpha$ for some $\alpha \leqslant 1$. For a solution with a $\chi^2 = \epsilon^2$, there is a probability α that pure noise gives a residual smaller than or equal to the observed residual n^*, and a probability $1-\alpha$ that noise gives a larger residual. Too small an α would thus induce possible noise over-fitting, i.e. inclusion of part of the noise in the reconstruction. These considerations might of course be generalized to other kinds of noise distributions.

The inverse problem being ill-posed, many signals may formally satisfy measurement constraints such as (9). In general, the problem may only find a unique solution x^*, as close as possible to the true signal x, through a regularization scheme which should encompass enough prior information on the original signal. All possible image reconstruction algorithms will essentially be distinguished through the kind of regularization considered.

2.3 Standard imaging techniques

The general inverse problem (5) is to be considered if one wishes to undo the multiplication by the illumination function and to recover the original signal x on the given field of view. In practice, the reconstruction is usually considered for the original image I already multiplied by the illumination function A, whose sampled values are $\bar{x} = Dx \in \mathbb{R}^N = \{\bar{x}_i = a_i x_i\}_{1\leqslant i\leqslant N}$. In this setting the inverse problem reads as

$$y = \bar{\Phi}_{\mathrm{ri}}\bar{x} + n, \tag{10}$$

with a sensing matrix $\bar{\Phi}_{\mathrm{ri}}$ strictly implementing a convolution:

$$\bar{\Phi}_{\mathrm{ri}} = MF. \tag{11}$$

Firstly, the most standard and otherwise already very effective image reconstruction algorithm from visibility measurements is called CLEAN. It approaches the image reconstruction in terms of the corresponding deconvolution problem in real space (Högbom 1974; Schwarz 1978; Thompson et al. 2004). In standard vocabulary, the inverse transform of the Fourier measurements with all non-observed visibilities set to zero is called the dirty image. Its sampled values $\bar{x}^{(d)} \in \mathbb{R}^N = \{\bar{x}_i^{(d)}\}_{1\leqslant i\leqslant N}$ are simply obtained by application of the adjoint sensing matrix to the observed visibilities: $\bar{x}^{(d)} = \bar{\Phi}_{\rm ri}^{\dagger} y$. The inverse transform of the binary mask identifying the interferometer is called the dirty beam. Its sampled values $d \in \mathbb{R}^N = \{d_i\}_{1\leqslant i\leqslant N}$ follow from the application of the adjoint sensing matrix to a vector of unit values $1_m \in \mathbb{R}^m$: $d = \bar{\Phi}_{\rm ri}^{\dagger} 1_m$. The inverse transform of the noise n with all non-observed visibilities set to zero defines an alternative expression of the noise in real space. Again its sampled values $n^{(d)} \in \mathbb{R}^N = \{n_i^{(d)}\}_{1\leqslant i\leqslant N}$ are simply obtained by application of the adjoint sensing matrix to the noise realization: $n^{(d)} = \bar{\Phi}_{\rm ri}^{\dagger} n$. The inverse problem (10) can thus be rephrased by expressing the dirty image as the convolution of the original image with the dirty beam, plus the noise:

$$\bar{x}^{(d)} = d \star \bar{x} + n^{(d)}. \tag{12}$$

CLEAN is a non-linear deconvolution method relying on this relation and working by local iterative beam removal. At each iteration, the point in real space is identified where a residual image, initialized to the dirty image, takes its maximum absolute value. The beam is removed at that point with the correct amplitude to produce the residual image for the next iteration. Simultaneously the maximum absolute value observed renormalized by the central value of the beam is added at the same point in the approximation image, initialized to a null image. This procedure assumes that the original signal is a sum of Dirac spikes. A sparsity or compressibility prior on the original signal in real space is implicitly introduced so that its energy is concentrated at specific locations. On the contrary, the Gaussian noise should be distributed everywhere on the image and should not significantly affect the selection of points in the iterations. This underlying sparsity hypothesis serves as a regularization of the inverse problem.

A loop gain factor γ is generally introduced in the procedure which defines the fraction of the beam considered at each iteration. Values γ around a few tenths are usually used which allow for a more cautious consideration of the sidelobes of the dirty beam. The overall procedure is greatly enhanced by this simple improvement, albeit at high computational cost. In a statistical sense, the stopping criterion for the iteration procedure should be set in terms of relation (9). However, the procedure is known to be slow and the algorithm is often stopped after an arbitrary number of iterations.

Various weighting schemes can be applied to the binary mask in Fourier. Natural weighting simply corresponds to replace the unit values by the inverse variance of the noise affecting the corresponding visibility measurement. This corresponds to a standard matched filtering operation allowing the maximization of the signal-to-noise ratio of the dirty image before deconvolution. So-called uniform and robust weightings can notably be used to correct for the non-uniformity of the Fourier coverage associated with the measured visibilities and to reduce the sidelobes of the dirty beam in real space. Multi-scale versions of this method were also developed (Cornwell 2008).

CLEAN and multi-scale versions may actually be formulated in terms of the well-known matching pursuit (MP) procedure (Mallat & Zhang 1993; Mallat 1998). The corresponding MP algorithm simply uses a circulant dictionary for which the projection on atoms corresponds to the convolution with the dirty beam. The loop gain factor may also be trivially introduced in this context.

Secondly, another approach to the reconstruction of images from visibility measurements is MEM. In contrast to CLEAN, MEM solves a global optimization problem in which the inverse problem (10) is regularized by the introduction of an entropic prior on the signal (Ables 1974; Gull & Daniell 1999; Cornwell & Evans 1985; Gull & Skilling 1999). For positive signals, the relative entropy function between a sampled signal $\bar{x} \in \mathbb{R}^N = \{\bar{x}_i\}_{1\leqslant i\leqslant N}$ and a model $z \in \mathbb{R}^N = \{z_i\}_{1\leqslant i\leqslant N}$ takes the simple form

$$S\left(\bar{x}, z\right) = -\sum_{i}^{N} \bar{x}_i \ln \frac{\bar{x}_i}{z_i}. \tag{13}$$

This function is always negative and takes its maximum null value when $\bar{x} = z$. In the absence of a precise knowledge of the signal $\bar{x}$, z is set to a vector of constant values. In such a case, maximizing the entropy prior promotes smoothness of the reconstructed image.

The MEM problem is the unconstrained optimization problem defined as the minimization of a functional corresponding to the sum of the relative entropy S and the χ^2:

$$\min_{\bar{x}' \in \mathbb{R}^N} \left[\frac{1}{2}\chi^2\left(\bar{x}'; \bar{\Phi}_{\rm ri}, y\right) - \tau S\left(\bar{x}', z\right)\right], \tag{14}$$

for some suitably chosen regularization parameter $\tau > 0$. In general, the minimization thus requires a trade-off between χ^2 minimization, and relative entropy maximization.

Notice that the definition (13) may easily be generalized for non-positive signals. A multi-scale version of MEM was also defined. It considers that the original image may have an efficient representation in terms of its decomposition in a wavelet basis. The entropy is then defined directly on the wavelet coefficients of the signal (Maisinger et al. 1999).

For completeness we finally quote the WIPE reconstruction procedure which also solves a global minimization problem, but in which the inverse problem (10) is regularized by the introduction of a smoothness prior on the part of the signal whose Fourier support corresponds to the non-probed spatial frequencies. This corresponds to minimize the χ^2 after assigning a null value to all initially non-observed visibilities (Lannes et al. 1994, 1996).

In conclusion, CLEAN is a local iterative deconvolution technique, while MEM and WIPE are reconstruction techniques based on global minimization problems. All three approaches are flexible enough to consider various bases (Dirac, wavelet, etc.) where a majority of natural signals can have a sparse or compressible representation. CLEAN also implicitly assumes the sparsity of the signal in the reconstruction procedure. But none of these methods explicitly imposes the sparsity or compressibility prior on the reconstruction. This precise gap is notably bridged by the imaging techniques defined in the framework of the compressed sensing theory.

3 COMPRESSED SENSING

In this section we define the general framework of the theory of compressed sensing and quote its essential impact beyond the Nyquist-Shannon sampling theorem. We then describe the restricted isometry property that the sensing basis needs to satisfy so that sparse and compressible signals may be accurately recovered through a global optimization problem. We finally discuss the idea that incoherence of the sensing and sparsity or compressibility bases as well as randomness of the measurements are the key properties to ensure this restricted isometry.

3.1 Beyond Nyquist-Shannon

In the framework of compressed sensing the signals probed are firstly assumed to be sparse or compressible in some basis. Technically, we consider a real signal identified by its Nyquist-Shannon sampling as $x \in \mathbb{R}^N = \{x_i\}_{1\leqslant i\leqslant N}$. A real basis $\Psi \in \mathbb{R}^{N\times T} = \{\Psi_{iw}\}_{1\leqslant i\leqslant N;1\leqslant w\leqslant T}$ is defined, which may be either orthogonal, with $T = N$, or redundant, with $T > N$ (Rauhut et al. 2008). The decomposition $\alpha \in \mathbb{R}^T = \{\alpha_w\}_{1\leqslant w\leqslant T}$ of the signal defined by

$$x = \Psi\alpha, \tag{15}$$

is sparse or compressible in the sense that it only contains a small number $K \ll N$ of non-zero or significant coefficients respectively. The signal is then assumed to be probed by m real linear measurements $y \in \mathbb{R}^m = \{y_r\}_{1\leqslant r\leqslant m}$ in some real sensing basis $\Phi \in \mathbb{R}^{m\times N} = \{\Phi_{ri}\}_{1\leqslant r\leqslant m;1\leqslant i\leqslant N}$ and possibly affected by independent and identically distributed noise $n \in \mathbb{R}^m = \{n_r\}_{1\leqslant r\leqslant m}$:

$$y = \Theta\alpha + n \text{ with } \Theta = \Phi\Psi \in \mathbb{R}^{m\times T}. \tag{16}$$

This number m of constraints is typically assumed to be smaller than the dimension N of the vector defining the signal, so that the inverse problem (16) is ill-posed.

In this context, the theory of compressed sensing defines the explicit restricted isometry property (RIP) that the matrix Θ should satisfy in order to allow an accurate recovery of sparse or compressible signals (Candès et al. 2006a,b; Candès 2006). In that regard, the theory offers multiple ways to design suitable sensing matrices Φ from properties of incoherence with Ψ and randomness of the measurements. It shows in particular that a small number of measurements is required relative to a naive Nyquist-Shannon sampling: $m \ll N$. The framework also defines a global minimization problem for the signal recovery called Basis Pursuit (BP). This problem regularizes the originally ill-posed inverse problem by an explicit sparsity or compressibility prior on the signal. The corresponding solution may be obtained through convex optimization. Alternative global minimization problems may also be designed.

3.2 Restricted isometry and Basis Pursuit

Let us primarily recall that the ℓ_p norm of a real vector $u \in \mathbb{C}^Q = \{u_l\}_{1\leqslant l\leqslant Q}$ is defined for any $p \in \mathbb{R}_+$ as $||u||_p \equiv (\sum_{l=1}^{Q} |u_l|^p)^{1/p}$, where $|u_l|$ stands for the absolute value of the component u_l. The well-known ℓ_2 norm is to the square-root of the sum of the absolute values squared of the vector components.

By definition the matrix Θ satisfies a RIP of order K if there exists a constant $\delta_K < 1$ such that

$$(1-\delta_K)\,||\alpha_K||_2^2 \leqslant ||\Theta\alpha_K||_2^2 \leqslant (1-\delta_K)\,||\alpha_K||_2^2, \tag{17}$$

for all vectors α_K containing at maximum K non-zero coefficients.

The ℓ_1 norm of the vector $\alpha \in \mathbb{R}^T = \{\alpha_w\}_{1\leqslant w\leqslant T}$ is simply defined as the sum of the absolute values of the vector components:

$$||\alpha||_1 \equiv \sum_{w=1}^{T} |\alpha_w|. \tag{18}$$

From a Bayesian point of view, this ℓ_1 norm may be seen as the negative logarithm of a Laplacian prior distribution on each independent component of α. For comparison the square of the ℓ_2 norm may be seen as the negative logarithm of a Gaussian prior distribution. It is well-known that a Laplacian distribution is highly peaked and bears heavy tails, relative to a Gaussian distribution. This corresponds to say that the signal is defined by only a small number of significant coefficients, much smaller than a Gaussian signal would be. In other words the representation α of the signal x in the sparsity or compressibility basis Ψ is indeed sparse or compressible if it follows such a prior. Finding the α' that best corresponds to this prior requires to maximize its Laplacian probability distribution, or equivalently to minimize the ℓ_1 norm. Notice that this conclusion also follows from a pure geometrical argument in $\mathbb{R}^T$ (Candès et al. 2006b; Baraniuk 2007).

A constrained optimization problem explicitly regularized by a ℓ_1 sparsity prior can be defined. This so-called Basis Pursuit denoise (BP$_\epsilon$) problem is the minimization of the ℓ_1 norm of α' under a constraint on the ℓ_2 norm of the residual noise:

$$\min_{\alpha'\in\mathbb{R}^T} ||\alpha'||_1 \text{ subject to } ||y - \Theta\alpha'||_2 \leqslant \epsilon. \tag{19}$$

Let us recall that the noise was assumed to be identically distributed. Consequently, considering Gaussian noise, the ℓ_2 norm term in the BP$_\epsilon$ problem is identical to the condition (9), for ϵ^2 corresponding to some suitable percentile of the χ^2 distribution with m degrees of freedom governing the noise level estimator. This BP$_\epsilon$ problem is solved by application of non-linear and iterative convex optimization algorithms (Combettes & Pesquet 2008; van den Berg & Friedlander 2008). In the absence of noise, the BP$_\epsilon$ problem is simply called Basis Pursuit (BP). If the solution of the BP$_\epsilon$ problem is denoted α^* then the corresponding synthesis-based signal reconstruction reads, from (15), as $x^* = \Psi\alpha^*$.

Compressed sensing shows that if the matrix Θ satisfies a RIP of order $2K$ with some suitable constant $\delta_{2K} < \sqrt{2} - 1$ (Candès 2008), then the solution x^* of the BP$_\epsilon$ problem provides an accurate reconstruction of a signal x that is sparse or compressible with K significant coefficients. The reconstruction may be said to be optimal in that exactly sparse signals are recovered exactly through BP in the absence of noise: $x^* = x$. Moreover strong stability results exist for compressible signals in the presence of noise. In that case, the ℓ_2 norm of the difference between the representation α of the signal in the sparsity or compressibility basis and its reconstruction α^* is bounded by the sum of two terms. The first term is due to the noise and is proportional to ϵ. The second term is due to the non-exact sparsity of a compressible signal and is proportional to the ℓ_1 norm of the difference between α and the approximation α_K defined by retaining only its K largest components and sending all other values to zero. In this context, one has

$$||\alpha - \alpha^*||_2 \leqslant C_{1,K}\epsilon + C_{2,K}\frac{||\alpha - \alpha_K||_1}{\sqrt{K}}, \tag{20}$$

for two known constants $C_{1,K}$ and $C_{2,K}$ depending on δ_{2K}. For instance, when $\delta_{2K} = 0.2$, we have $C_{1,K} = 8.5$ and $C_{2,K} = 4.2$ (Candès et al. 2006b; Candès 2008). In an orthonormal basis Ψ this relation represents an explicit bound on the ℓ_2 norm of the difference between the signal x itself and its reconstruction x^* as $||x - x^*||_2 = ||\alpha - \alpha^*||_2$. Moreover $x_K = \Psi\alpha_K$ then represents the best sparse approximation of x with K terms, in the sense that $||x - x_K||_2$ is minimum.

The constrained BP$_\epsilon$ problem may also be rephrased in terms of an unconstrained minimization problem for a functional defined as the sum of the ℓ_1 norm of α' and the ℓ_2 norm of the residual noise:

$$\min_{\alpha'\in\mathbb{R}^T}\left[\frac{1}{2}||y - \Theta\alpha'||_2^2 + \tau||\alpha'||_1\right], \tag{21}$$

for some suitably chosen regularization parameter $\tau > 0$. For each value of ϵ, there exists a value τ such that the solutions of the constrained and unconstrained ℓ_1 sparsity problems are identical (van den Berg & Friedlander 2008). From a Bayesian point of view, this minimization is then equivalent to maximum a posteriori (MAP) estimation for a signal with Laplacian prior distribution in the sparsity or compressibility basis, in the presence of Gaussian noise.

Finally, alternative minimization problems may be defined for the recovery. Firstly, a ℓ_p norm with $0 < p \leqslant 1$ may for example be substituted for the ℓ_1 norm in the definition of the minimization problem. From a Bayesian point of view, the ℓ_p norm to the power p may be seen as the negative logarithm of a prior distribution identified as a generalized Gaussian distribution (GGD). Such distributions are even more highly peaked and bear heavier tails than a Laplacian distribution and thus promote stronger compressibility of the signals. Theoretical results hold for such ℓ_p norm minimization problems when a RIP is satisfied (Foucart & Lai 2008). Such problems are non-convex but can be solved iteratively by convex optimization algorithms performing re-weighted ℓ_1 norm minimization (Candès et al. 2008; Davies & Gribonval 2008; Foucart & Lai 2008; Chartrand & Yin 2007). Secondly, a TV norm may also be substituted for the ℓ_1 norm in the definition of the minimization problem for signals with sparse or compressible gradients. The TV norm of a signal is simply defined as the ℓ_1 norm of the magnitude of its gradient (Rudin et al. 1992). A theoretical result of exact reconstruction holds for such TV norm minimization problems in the case of Fourier measurements of signals with exactly sparse gradients in the absence of noise (Candès et al. 2006a). But no proof of stability relative to noise and non-exact sparsity exists at the moment. Such minimization is also accessible through an iterative scheme from convex optimization algorithms (Candès & Romberg 2005).

This flexibility in the definition of the optimization problem is a first important manifestation of the versatility of the compressed sensing theory, and of the convex optimization scheme. It opens the door to the definition a whole variety of powerful image reconstruction techniques that may take advantage of some available specific prior information on the signal under scrutiny beyond its generic sparsity or compressibility.

3.3 Incoherence and randomness

The issue of the design of the sensing matrix Φ ensuring the RIP for $\Theta = \Phi\Psi$ is of course fundamental. One can actually show that incoherence of Φ with the sparsity or compressibility basis Ψ and randomness of the measurements will ensure that the RIP is satisfied with overwhelming probability, provided that the number of measurements is large enough relative to the sparsity K considered (Candès et al. 2006b; Candès 2006). In this context, the variety of approaches to design suitable sensing matrices is a second form of the versatility of the compressed sensing framework.

As a first example, the measurements may be drawn from a Gaussian matrix Φ with purely random real entries, in which case the RIP is satisfied if

$$K \leqslant \frac{Cm}{\ln(N/m)}, \tag{22}$$

for some constant C. The most recent result provides a value $C \simeq 0.5$, hence showing that the required redundancy of measurements m/K is very small (Donoho & Tanner 2009).

As a second example of interest for radio interferometry, the measurements may arise from a uniform random selection of Fourier frequencies. In this case, the precise condition for the RIP depends on the degree of incoherence between the Fourier basis and the sparsity or compressibility basis. If the unit-normed basis vectors corresponding to the lines of F and the columns of Ψ are denoted $\{f_e\}_{1\leqslant e\leqslant N}$ and $\{\psi_{e'}\}_{1\leqslant e'\leqslant T}$, the mutual coherence μ of the bases may be defined as their maximum scalar product:

$$\mu = \sqrt{N} \max_{e,e'} |\langle f_e|\psi_{e'}\rangle|. \tag{23}$$

The RIP is then satisfied if

$$K \leqslant \frac{C'm}{\mu^2 \ln^4 N}, \tag{24}$$

for some constant C'. As the incoherence is maximum between the Fourier and real spaces with $\mu = 1$, the lowest number of measurements would be required for a signal that is sparse in real space. Notice that a factor $\ln N$ instead of $\ln^4 N$ in condition (24) was not proven but conjectured, suggesting that a lower number of measurements would still ensure the RIP. In that regard, empirical results (Lustig et al. 2007) suggest that ratios m/K between 3 and 5 already ensure a reconstruction quality through BP$_\epsilon$ that is equivalent to the quality ensured by (20).

Let us also emphasize that the TV norm minimization is often used from Fourier measurements of signals with sparse or compressible gradients. As already stated no stability result such as (20) was proven for the reconstruction provided by this minimization scheme. Empirical results suggest however that TV norm minimization provides the same quality of reconstruction as BP$_\epsilon$ for the same typical ratios m/K between 3 and 5 (Candès & Romberg 2005; Lustig et al. 2007).

4 APPLICATIONS

In this section, we firstly comment on the exact compliance of radio interferometric measurements with compressed sensing. We then consider simulations of two kinds of signals for reconstruction from visibility measurements: an intensity field of compact astrophysical objects and a signal induced by cosmic strings in the temperature field of the cosmic microwave background (CMB) radiation. Relying on the versatility of the convex optimization scheme, enhanced minimization problems are defined in the compressed sensing perspective through the introduction of specific prior information on the signals. The reconstruction performance is studied in comparison both with the standard BP$_\epsilon$ reconstructions in the absence of specific priors and with the CLEAN reconstruction.

4.1 Interferometric measurements and compressed sensing

In the context of compressed sensing, the sensing matrix needs to satisfy the RIP. If Fourier measurements are considered, this requirement may be reached through a uniform random selection of a low number of Fourier frequencies. In the context of radio interferometry, realistic visibility distributions are deterministic, i.e. non-random, superpositions of elliptical distributions in the Fourier plane of the image to reconstruct. However, the structure of the Fourier sampling is extremely dependent on the specific configuration of the radio telescope array under consideration. Visibilities from various interferometers may be combined, as well as visibilities from the same interferometer with different pointing directions in the mosaicking technique (Thompson et al. 2004). From this point of view the realistic visibility distributions themselves are rather flexible. Moreover, the standard uniform weighting of the visibilities may be used to provide uniformity of the effective measurement density in the Fourier plane. Correctly studied realistic distributions might thus not be so far from complying exactly with the compressed sensing requirements. Finally, it was recently suggested that specific deterministic distributions of a low number of linear measurements might in fact allow accurate signal reconstruction in the context of compressed sensing (Matei & Meyer 2008).

Nonetheless, modifications of radio interferometric measurements might be conceived in order to comply exactly with standard compressed sensing results. To this end, one might want to introduce randomness in the visibility distribution. Formally, random repositioning of the telescopes during observation or random integration times for the definition of individual visibilities could provide important advances in that direction. Also notice that compressed sensing does not require that measurements be identified to Fourier coefficients of the signal. The versatility of the framework relative to the design of suitable sensing matrices might actually be used to define generalized radio interferometric measurements, beyond standard visibilities, ensuring that the RIP is explicitly satisfied. In this perspective, direct modifications of the acquisition process through a scheme similar to spread spectrum techniques (Naini et al. 2009) or coded aperture techniques (Marcia & Willett 2008) could also provide important advances.

In the following applications we simply consider standard visibility measurements. We assume generic interferometric configurations characterized by uniform random selections of visibilities.

4.2 Experimental set up

We consider two kinds of astrophysical signals I that are sparse in some basis, and for which specific prior information is available. For each kind of signal, 30 simulations are considered. Observations of both kinds of signals are simulated for five hypothetical radio interferometers unaffected by instrumental noise, assuming that the conditions under which relation (3) holds are satisfied. The field of view observed on the celestial sphere by the interferometers is limited by a Gaussian illumination function A with a full width at half maximum (FWHM) of 40 arcminutes of angular opening. The original signals considered are defined as sampled images with $N = 256 \times 256$ pixels on a total field of view of $1.8^\circ \times 1.8^\circ$.

The first kind of signal consists of a compact object intensity field in which the astrophysical objects are represented as a superposition of elongated Gaussians of various scales in some arbitrary intensity units. The important specific prior information in this case is the positivity of the signal. The second kind of signal is of particular interest for cosmology. It consists of temperature steps in μK induced by topological defects such as cosmic strings in the zero-mean perturbations of the CMB. The string network of interest can be mapped as the magnitude of the gradient of the string signal itself. The essential specific prior information in this case resides in the fact that the statistical distribution of a string signal may be well modelled in wavelet space. One simulation of a compact object intensity field and the magnitude of the gradient of one simulation of a string signal are represented in Figure 1, after multiplication by the illumination function.

As discussed already, we assume uniform random selections of visibilities. The five interferometers considered identified by an index c with $1 \leqslant c \leqslant 5$ only differ by their Fourier coverage. This coverage is defined by the $m/2$ randomly distributed frequencies probed in one half of the Fourier plane, corresponding to m real Fourier coefficients as: $m/N = 5c/100$. For each configuration, the general inverse problem is the one posed in (5) with the sensing matrix $\Phi = \Phi_{\rm ri}$ defined in (6) if one wishes to undo the multiplication by the illumination function and to recover the original signal x. The inverse problem (10) applies with the sensing matrix $\Phi = \bar{\Phi}_{\rm ri}$ defined in (11) if one wishes to recover $\bar{x}$.

For each reconstruction, we compare the performance of the Basis Pursuit approaches enhanced by the inclusion of specific prior signal information in the minimization problem, with both the standard BP$_\epsilon$ or BP performance, and the CLEAN performance. As the signals considered are sparse or compressible in some basis, we do not consider any MEM or WIPE reconstruction, which disregard the sparsity information. The performance of the algorithms compared is evaluated through the signal-to-noise ratio (SNR) of the reconstruction for the compact object intensity field, and through the SNR of the magnitude of the gradient of the reconstruction for the string signal. The SNR of a reconstructed signal $\overline{s}$ relative to an original signal s is technically defined as

$$\mathrm{SNR}^{(s,\overline{s})} = -20 \log_{10} \frac{\sigma^{(s-\overline{s})}}{\sigma^{(s)}}, \quad (25)$$

where $\sigma^{(s-\overline{s})}$ and $\sigma^{(s)}$ stand for the sampled standard deviations of the residual signal $s - \overline{s}$ and of the original signal s, respectively. It is consequently measured in decibels (dB).

As far as the computation complexity of the algorithms is concerned, notice that both CLEAN and the various Basis Pursuit algorithms considered share the same scaling with N at each iteration. This scaling is driven by the complexity of the FFT, i.e. $\mathcal{O}(N \log N)$. The number of iterations required by each algorihm is therefore critical in a comparison of computation times.

4.3 Compact object intensity field

Each simulation of the compact object intensity field consists of 100 Gaussians with random positions and orientations, random amplitudes in the range $[0, 1]$ in the chosen intensity units, and random but small scales identified by standard deviations along each basis direction in the range $[1, 4]$ in number of pixels. Given their structure, such signals are probably optimally modelled by sparse approximations in some wavelet basis. But as the maximum possible incoherence with Fourier space is reached from real space, we chose the sparsity or compressibility basis to be the Dirac basis, i.e. $\Psi = \mathbb{I}_{N^{1/2} \times N^{1/2}}$. For further simplification of the problem we consider the inverse problem (10) with the sensing matrix $\bar{\Phi}_{\rm ri}$, for reconstruction of the original signal $\bar{x}$ multiplied by the illumination function.

As no noise is considered, a BP problem is considered in a standard compressed sensing approach. However, the prior knowledge of the positivity of the signal also allows one to pose an enhanced BP+ problem as:

$$\min_{\bar{x}' \in \mathbb{R}^N} ||\bar{x}'||_1 \text{ subject to } y = \bar{\Phi}_{\rm ri} \bar{x}' \text{ and } \bar{x}' \geqslant 0. \quad (26)$$

Notice that no theoretical recovery result was yet provided for such a problem in the described framework of compressed sensing. But the performance of this approach for the problem considered is assessed on the basis of the simulations. The positivity prior is easily incorporated into a convex optimization solver based on proximal operator theory (Moreau 1962). The Douglas-Rachford splitting method (Combettes & Pesquet 2008) guarantees that such an additional convex constraint is inserted naturally in an efficient iterative procedure finding the global minimum of the BP+ problem. For simplicity, the stopping criterion of the iterative process is here set in terms of the number of iterations: 10^4.

The BP+ reconstruction of the original signal $\bar{x}$ reported in Figure 1 is also represented in the figure for the configuration $c = 2$. For comparison, the dirty image $\bar{x}^{(d)}$ used in CLEAN and obtained by simple application of the adjoint sensing matrix $\bar{\Phi}_{\rm ri}^\dagger$ to the observed visibilities is also represented. The mean SNR and

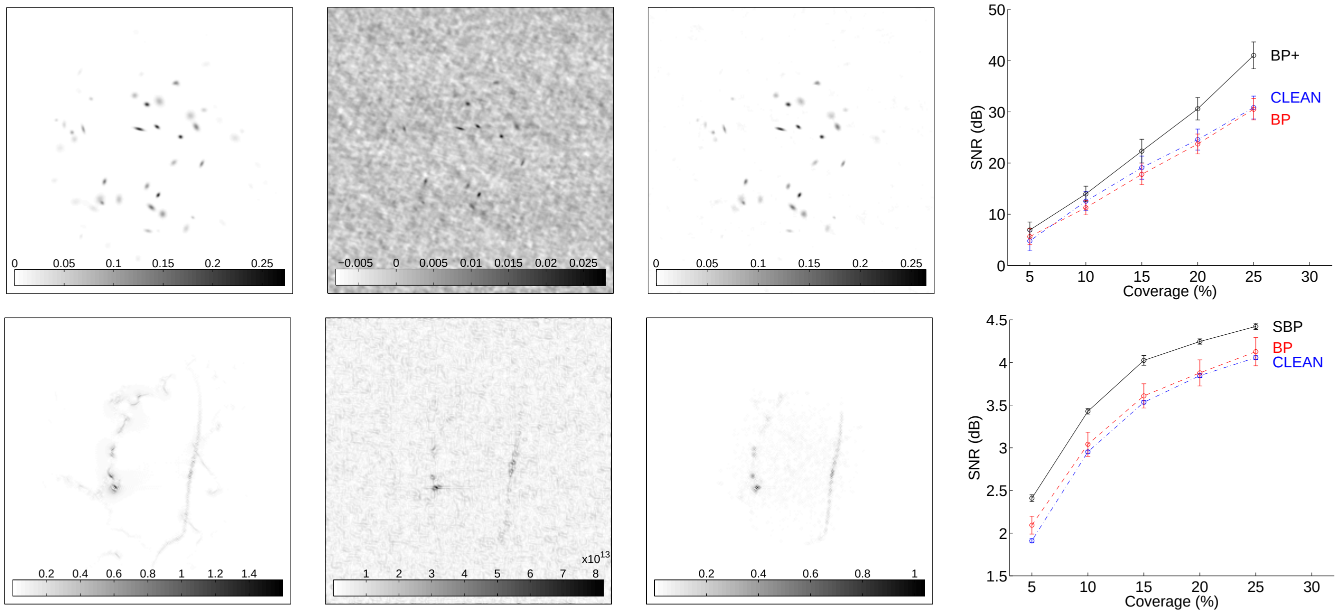

Figure 1. Top panels: compact object intensity field in some arbitrary intensity units. The original signal multiplied by the illumination function $\bar{x}$ is reported (left), as well as the dirty image $\bar{x}^{(d)}$ (center left) and the BP+ reconstruction of $\bar{x}$ (center right), for the interferometric configuration $c = 2$. The graph of the mean SNR with 1σ error bars over 30 simulations is also reported for the CLEAN, BP, and BP+ reconstructions of $\bar{x}$ as a function of the Fourier coverage identifying the interferometric configurations (extreme right). Bottom panels: string signal in the CMB in μK. The magnitude of the gradient of the original signal x re-multiplied by the illumination function is reported (left), as well as the dirty image $\bar{x}^{(d)}$ (center left) and the SBP$_\epsilon$ reconstruction of x re-multiplied by the illumination function (center right), for the interferometric configuration $c = 2$. The graph of the mean SNR with 1σ error bars over 30 simulations is also reported for the CLEAN reconstruction, and for the BP$_\epsilon$ and SBP$_\epsilon$ reconstructions re-multiplied by the illumination function, as a function of the Fourier coverage identifying the interferometric configurations (extreme right).

corresponding one standard deviation (1σ) error bars over the 30 simulations are reported in Figure 1 for the CLEAN reconstruction of $\bar{x}$ with $\gamma = 0.1$, and for the BP and BP+ reconstructions of $\bar{x}$, as a function of the Fourier coverage identifying the interferometric configurations. All obviously compare very favorably relative to the SNR of $\bar{x}^{(d)}$, not reported on the graph. One must acknowledge the fact that BP and CLEAN provide relatively similar qualities of reconstruction. However, the BP reconstruction is actually achieved much more rapidly than the CLEAN reconstruction, both in terms of number of iterations and computation time. This highlights the fact that the BP approach may in general be computationally much less expensive. The BP+ reconstruction exhibits a significantly better SNR than the BP and CLEAN reconstructions. The main outcome of this analysis thus resides in the fact that the inclusion of the positivity prior on the signal significantly improves reconstruction. For completeness, let us mention that it was suggested decades ago that CLEAN can be understood as some approximation of what we called the BP+ approach (Marsh & Richardson 1987).

Notice that the sparsity or compressibility basis is orthonormal and the error $||\bar{x} - \bar{x}^*||_2$ in the BP reconstruction $\bar{x}^*$ of $\bar{x}$ is theoretically bounded by (20) with $\epsilon = 0$. Assuming saturation of this bound, the SNR of the BP reconstruction allows the estimation of the maximum sparsity K of the best sparse approximation $\bar{x}_K$ of $\bar{x}$. Preliminary analysis from the mean SNR of reconstructions over the simulations considered suggests that ratios $m/K \simeq 5$ hold for each of the values of m associated with the five interferometric configurations probed. This result appears to be in full coherence with the accepted empirical ratios quoted above (Lustig et al. 2007).

4.4 String signal in the CMB

The CMB signal as a whole is a realization of a statistical process. In our setting, the zero-mean temperature perturbations considered in μK may be modelled as a linear superposition of the non-Gaussian string signal x made up of steps and of a Gaussian component g seen as noise. The power spectrum of this astrophysical noise is set by the concordance cosmological model. We only include here the so-called primary CMB anisotropies (Hammond et al. 2008). The typical number, width and spatial distribution of long strings or string loops in a given field of view are also all governed by the concordance cosmological model. Our 30 simulations of the CMB signal are built as a superposition of a unique realistic string signal simulation borrowed from Fraisse et al. (2008) with 30 simulations of the Gaussian correlated noise. The string tension ρ, a dimensionless number related to the mass per unit length of string, is up to some extent a free parameter of the model. This tension sets the overall amplitude of the signal and needs to be evaluated from observations. For the sake of the present analysis, we only study the string signal for one realistic value $\rho = 3.2 \times 10^{-8}$, which technically fixes the SNR of the observed string signal buried in the astrophysical noise. This value is assessed prior to any signal reconstruction, by fitting the power spectrum of the data to the sum of the power spectra of the signal and noise on the frequencies probed (Hammond et al. 2008). This estimation may be considered as very precise at the tension of interest and is not to be considered as a significant source of error in the subsequent reconstruction.

In this context, preliminary analysis of 16 independent realistic simulations of a string signal, also from Fraisse et al. (2008), allows one to show that the random process from which the string signal arises is well modelled by GGD's in wavelet space (Hammond et al. 2008). We consider a redundant steerable wavelet basis $\Psi_{\rm s}$ with 6 scales j ($1 \leqslant j \leqslant 6$) including low pass and high pass axisymmetric filters, and four intermediate scales defining steerable wavelets with 6 basis orientations q ($1 \leqslant q \leqslant 6$) (Simoncelli & Freeman 1995). By statistical isotropy, the GGD priors π_j for a wavelet coefficient α'_w only depend on the scale:

$$\pi_j\left(\alpha_w\right) \propto \exp\left[-\left|\frac{\alpha_w}{\rho u_j}\right|^{v_j}\right], \tag{27}$$

where w is to be thought of as a multi-index identifying a coefficient at given scale j, position i, and orientation q. Assuming independence of the wavelet coefficients, the total prior probability distribution of the signal is simply the product of the probability distributions for each value of w, which reads as

$$\pi\left(\alpha\right) \propto \exp -||\alpha||_{\rm s}, \tag{28}$$

for a "s" norm

$$||\alpha||_{\rm s} \equiv \sum_w \left|\frac{\alpha_w}{\rho u_j}\right|^{v_j}. \tag{29}$$

The exponent parameters v_j are called GGD shape parameters and can be considered as a measure of the compressibility of the underlying distribution. Values close to 0 yield very peaked probability distributions with heavy tails relative to Gaussian distributions, i.e. very compressible distributions. The list of these values at all scales reads as: $\{v_1 = 0.43, v_2 = 0.39, v_3 = 0.47, v_4 = 0.58, v_5 = 0.76, v_6 = 1.86\}$. The signal is thus understood as being well modelled by a very compressible expansion in its wavelet representation and we choose the corresponding redundant basis as the sparsity or compressibility basis for the inverse problem: $\Psi = \Psi_{\rm s}$. The list values of the GGD scale parameters u_j identifying the variances of the distributions at all scales reads as: $\{u_1 = 8.9 \times 10^{-3}, u_2 = 2.8 \times 10^{-3}, u_3 = 2.2 \times 10^{-2}, u_4 = 0.15, u_5 = 0.95, u_6 = 57\}$. In full generality we consider the general inverse problem (5) with the sensing matrix $\Phi_{\rm ri}$, for reconstruction of the original signal x non-multiplied by the illumination function.

Even in the absence of instrumental noise the measured visibilities thus follow from (16) with a noise term

$$n = \Phi_{\rm ri}\, g, \tag{30}$$

representing values of the Fourier transform of the astrophysical noise g multiplied by the illumination function. Discarding the very local correlations in the Fourier plane introduced by the illumination function, one may consider that the measurements are independent and affected by independent Gaussian noise realizations. The corresponding noise variance σ_r^2 on y_r with $1 \leqslant r \leqslant m$, is thus identified from the values of the known power spectrum of g.

A whitening matrix $W_{\rm cmb} \in \mathbb{R}^{m\times m} = \{(W_{\rm cmb})_{rr'} = \sigma_r^{-1}\delta_{rr'}\}_{1\leqslant r,r'\leqslant m}$ is introduced on the measured visibilities y, so that the corresponding visibilities $\tilde{y} = W_{\rm cmb}\, y$ are affected by independent and identically distributed noise, as required to pose a BP$_\epsilon$ problem. This operation corresponds to a matched filtering in the absence of which any hope of good reconstruction is vain. A BP$_\epsilon$ problem is thus considered after estimation of ρ. However, the prior statistical knowledge on the signal also allows one to pose an enhanced Statistical Basis Pursuit denoise (SBP$_\epsilon$) problem. It is defined as the minimization of the negative logarithm of the specific prior on the signal, i.e. the s norm of the vector of its wavelet coefficients, under the measurement constraint:

$$\min_{\alpha'\in\mathbb{R}^T} ||\alpha'||_{\rm s} \text{ subject to } ||\tilde{y} - W_{\rm cmb}\Phi_{\rm ri}\Psi_{\rm s}\alpha'||_2 \leqslant \epsilon. \tag{31}$$

Notice that the s norm is similar but still more general than a single ℓ_p norm and no theoretical recovery result was yet provided for such a problem in the framework of compressed sensing. Again, the performance of this approach for the problem considered is assessed on the basis of the simulations. Most shape parameters v_j are smaller than 1, which implies that the norm defined is not convex. We thus reconstruct the signal through the re-weighted ℓ_1 norm minimization described above (Candès et al. 2008). In this regard, we use the SPGL1 toolbox (van den Berg & Friedlander 2008)[4]. The value of ϵ^2 in the BP$_\epsilon$ and SBP$_\epsilon$ problems is taken to be around the 99$^{\rm th}$ percentile of the χ^2 with m degrees of freedom governing the noise level estimator. This value also serves as the stopping criterion for the CLEAN reconstruction.

The magnitude of the gradient of the SBP$_\epsilon$ reconstruction of the original signal x reported in Figure 1 is also represented in the figure for the configuration $c = 2$, after re-multiplication by the illumination function which sets the field of view of interest. For comparison, the magnitude of the gradient of the dirty image $\bar{x}^{(d)}$ used in CLEAN and obtained by simple application of the adjoint sensing matrix $\bar{\Phi}_{\rm ri}^{\dagger}$ to the observed visibilities is also represented.

The mean SNR and corresponding one standard deviation (1σ) error bars over the 30 simulations are reported in Figure 1 for the CLEAN reconstruction with $\gamma = 0.1$, and for the BP$_\epsilon$ and SBP$_\epsilon$ reconstructions re-multiplied by the illumination function, as a function of the Fourier coverage identifying the interferometric configurations. All obviously compare very favorably relative to the SNR of $\bar{x}^{(d)}$, not reported on the graph. One must still acknowledge the fact that BP$_\epsilon$ and CLEAN provide relatively similar qualities of reconstruction. The BP$_\epsilon$ reconstruction is achieved much more rapidly than the CLEAN reconstruction, highlighting the fact that the BP$_\epsilon$ approach may in general be computationally much less expensive. The SBP$_\epsilon$ reconstruction exhibits a significantly better SNR than the BP and CLEAN reconstructions.

Let us acknowledge the fact that the re-weighted ℓ_1 norm minimization of the SBP$_\epsilon$ approach proceeds by successive iterations of ℓ_1 norm minimization. This unavoidably significantly increases the computation time for reconstruction relative to the single ℓ_1 norm minimization of the BP$_\epsilon$ approach. Relying on the idea that the coefficients of the low pass filter do not significantly participate to the identification of the string network itself, our implementation of SBP$_\epsilon$ does not perform any re-weighting at the scale $j = 6$, where $v_6 = 1$ was thus assumed. This restriction allows one to keep SBP$_\epsilon$ computation times similar to those of CLEAN. Let us notice however that an even better SNR is obtained by correct re-weighting at $j = 6$, albeit at the cost of a prohibitive increase in computation time.

The main outcome of the analysis is twofold. Firstly, the presence of a whitening operation is essential when correlated noise is considered. Secondly, the inclusion of the prior statistical knowledge on the signal also significantly improves reconstruction.

5 CONCLUSION

Compressed sensing offers a new framework for image reconstruction in radio interferometry. In this context, the inverse problem for image reconstruction from incomplete and noisy Fourier measurements is regularized by the definition of global minimization problems in which a generic sparsity or compressibility prior is explic-

[4] http://www.cs.ubc.ca/labs/scl/spgl1/

itly imposed. These problems are solved through convex optimization. The versatility of this scheme also allows inclusion of specific prior information on the signal under scrutiny in the minimization problems. We studied reconstruction performances on simulations of an intensity field of compact astrophysical objects and of a signal induced by cosmic strings in the CMB temperature field, observed with very generic interferometric configurations. The BP$_\epsilon$ technique provides similar reconstruction performances as the standard matching pursuit algorithm CLEAN. The inclusion of specific prior information significantly improves the quality of reconstruction.

Further work by the authors along these lines is in preparation. In particular, a more complete analysis is being performed to estimate the lowest string tension down to which compressed sensing imaging techniques can reconstruct a string signal in the CMB, in more realistic noise and Fourier coverage conditions. In this case, given the compressibility of the magnitude of the gradient of the string signal itself, TV norm minimization also represents an interesting alternative to the SBP$_\epsilon$ problem proposed here.

ACKNOWLEDGMENTS

The authors wish to thank A. A. Fraisse, C. Ringeval, D. N. Spergel, and F. R. Bouchet for kindly providing string signal simulations, as well as M. J. Fadili for discussions on optimization by proximal methods. The authors also thank the reviewer T. J. Cornwell for his valuable comments. The work of Y. W. was funded by the Swiss National Science Foundation (SNF) under contract No. 200020-113353. Y. W. and L. J. are Postdoctoral Researchers of the Belgian National Science Foundation (F.R.S.-FNRS).

References

Ables, J. G., 1974, A&AS, 15, 383
Baraniuk R., 2007, IEEE Signal Proc. Magazine, 24, 118
Bobin J., Starck J.-L., Ottensamer R., 2008, IEEE Sel. Top. Signal Proc., 2, 718
Blythe J. H., 1957, MNRAS, 117, 644
Candès E. J., Romberg J., 2005, preprint (http://www.dsp.ece.rice.edu/cs/, January 2005)
Candès E. J., Romberg J., Tao T., 2006a, IEEE Trans. Inform. Theory, 52, 489
Candès E. J., Romberg J., Tao T., 2006b, Comm. Pure and Appl. Math., 59, 1207
Candès E. J., 2006, Proc. Int. Congress Math. Vol. 3. Euro. Math. Soc., p. 1433
Candès E. J., Wakin M., Boyd S., 2008, preprint (arXiv:0711.1612v1 [stat.ME])
Candès E. J., 2008, Compte Rendus de l'Academie des Sciences, Paris, Series I, 346, 589
Carilli C., Rawlings S., eds, 2004, New Astron. Rev., Vol. 48, Science with the Square Kilometre Array. Elsevier, Oxford
Chartrand R., Yin W., 2007, preprint (http://www.dsp.ece.rice.edu/cs/, 2007)
Combettes P. L., Pesquet J. C., 2007, IEEE Sel. Top. Signal Proc., 1, 564
Cornwell T. J., Evans K. F., 1985, A&A, 143, 77
Cornwell T. J., Golap K., Bhatnagar S., 2008, IEEE Sel. Top. Signal Proc., 2, 647
Cornwell T. J., 2008, preprint (arXiv:0806.2228v1 [astro-ph])
Davies M. E., Gribonval R., 2008, preprint (http://www.dsp.ece.rice.edu/cs/, July 2008)
Donoho D. L., 2006, IEEE Trans. Inform. Theory, 52, 1289
Donoho D. L., Tanner J., 2009, Journal of the AMS, 22, 1
Foucart S., Lai M.-J., 2008, preprint (http://www.dsp.ece.rice.edu/cs/, July 2008)
Fraisse A. A., Ringeval C., Spergel D. N., Bouchet F. R., 2008, Phys. Rev. D, 78, 043535
Gull S. F., Daniell G. J., 1978, Nat, 272, 686
Gull S. F., Skilling J., 1999. Quantified Maximum Entropy, MemSys5 Users' Manual. Maximum Entropy Data Consultants Ltd.
Hammond D. K., Wiaux Y., Vandergheynst P., 2008, preprint (arXiv:0811.1267v1 [astro-ph])
Högbom J. A., 1974, A&AS, 15, 417
Lannes A., Anterrieu E., Bouyoucef K., 1994, J. Mod. Optics., 41, 1537
Lannes A., Anterrieu E., Bouyoucef K., 1996, J. Mod. Optics., 43, 105
Levanda R., Leshem A., 2008, Proc. 25th Conv. IEEE Israel. IEEE Signal Proc. Soc., p. 716
Lustig M., Donoho D., Pauly J. M., 2007, Mag. Res. Medicine, 58, 1182
Maisinger K., Hobson M. P., Lasenby A. N., 2004, MNRAS, 347, 339
Mallat S. G., Zhang Z., 1993, IEEE Trans. Signal Proc., 41, 3397
Mallat S. G., 1998, A wavelet tour of signal processing. Academic Press, San Diego
Marcia R. F., Willett R. M. , 2008, Proc. IEEE Int. Conf. on Acoustics, Speech and Signal Proc.. IEEE Signal Proc. Soc., p. 833
Marsh K. A., Richardson J. M., 1987, A&A, 182, 174
Mary D., Michel O. J. J., 2007, Proc. GRETSI Coll., p. 733
Matei B., Meyer Y., preprint (http://www.dsp.ece.rice.edu/cs/, 2008)
McEwen J. D., Scaife A. M. M., 2008, MNRAS, 389, 1163
Moreau J. J., 1962, A&A, 255, 2897
Naini F. M., Gribonval R., Jacques L., Vandergheynst P., 2009, Proc. IEEE Int. Conf. on Acoustics, Speech and Signal Proc.. IEEE Signal Proc. Soc., in press
Potts D., Steidl G., Tasche M., 2001, in Benedetto J. J., Ferreira P. J. S. G., eds, Modern Sampling Theory: Mathematics and Applications. Birkhuser, Boston, p. 249
Rauhut H., Schnass K., Vandergheynst P., 2008, IEEE Trans. Inform. Theory, 54, 2210
Rudin L. I., Osher S., Fatemi E., 1992, Physica D, 60, 259
Ryle M., Vonberg D. D., 1946, Nat, 158, 339
Ryle M., Hewish A., Shakeshaft J. R., 1959, IRE Trans. Antennas Propag., 7, S120
Ryle M., Hewish A., 1960, MNRAS, 120, 220
Schwarz U. J., 1978, A&A, 65, 345
Simoncelli E. P., Freeman W. T., 1995, Proc. IEEE Int. Conf. Signal Proc. Vol. III. IEEE Signal Proc. Soc., p. 444
van den Berg E., Friedlander M. P., 2008, SIAM J. Sci. Comput., 31, 890
Thompson A. R., Moran J. M., Swenson Jr. G. W., 2004, Interferometry and Synthesis in Radio Astronomy. WILEY-VCH Verlag GmbH & Co. KGaA, Weinheim